

Chapter 2

Metallic Nanoparticles for Theranostics

Abstract Metallic NPs such as Au, Ag possess excellent surface plasmon resonance (SPR) optical properties that can be tuned from visible to near-infrared (500–1300 nm) which make them ideal candidate systems for theranostics applications.

Keyword Silver nanoparticles • Gold nanoparticles • Targeted drug delivery • Targeted gene delivery • Antimicrobial nanoparticles • Cancer therapy

Metallic NPs such as Au, Ag possess excellent surface plasmon resonance (SPR) optical properties that can be tuned from visible to near-infrared (500–1300 nm) which make them ideal candidate systems for theranostics applications.

2.1 Shape-Controlled Synthesis of Silver and Gold Nanoparticles

Silver NPs can be synthesized in different shapes such as cubes, triangles, wires and aligned wires (Fig. 2.1). Hydrothermal mediated synthesis of Ag NPs at 120 °C using a cationic surfactant (CTAB–cetyltrimethylammonium bromide) allowed for a shape-controlled assembly by varying initial concentrations of CTAB and [Ag (NH₃)₂]OH (Yu and Yam 2005). Interestingly, nanoplates or triangles of Ag have potential applications in Surface-Enhanced Raman Scattering (SERS) (Nie and Emory 1997) molecular detection, and photothermal-based therapies.

The reaction medium can also play a role in imparting shape-controlled synthesis of NPs. N,N-Dimethylformamide (DMF) has been shown to be a good reducing agent for Ag and Au NPs (Pastoriza-Santos and Liz-Marzán 2009). Both silver salt and poly(vinylpyrrolidone) (PVP) concentrations were found to be essential parameters for tuning particle shape (Pastoriza-Santos and Liz-Marzán 2002). The important role of PVP in providing colloidal stability and tuning the morphology of the particles has been well established. The seeded growth approach has proven to be versatile when DMF is used as a reducing agent and PVP as a stabilizer in

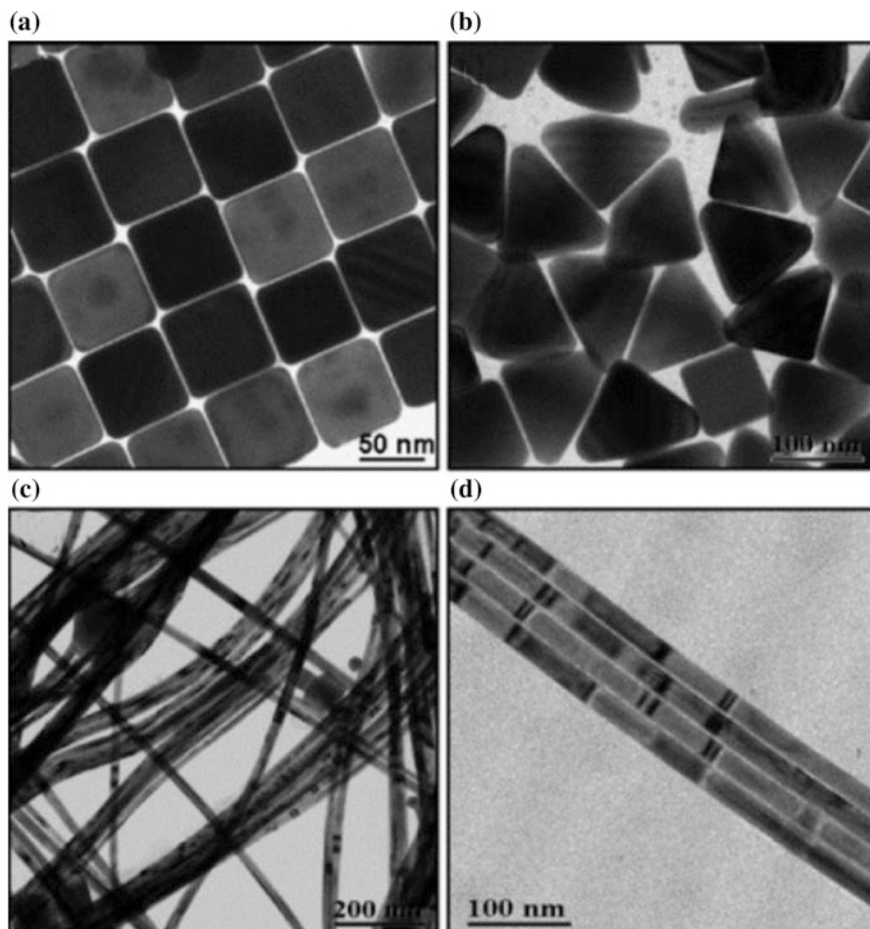


Fig. 2.1 TEM images of Ag NPs. **a** cubes, **b** triangles, **c** wires and **d** aligned wires (Yu and Yam 2005) (Copyright obtained)

dictating the uniform size Au and Ag NPs with various shapes (decahedra, octahedra, spheres, sharp rods, stars, etc.).

It is also possible to modulate the optical response of metal NPs through size and shape control (Fig. 2.2). When the particle size is increased, there is change in the absorption spectra (spectral red-shifts) for spheres (Fig. 2.1a) and decahedra (Fig. 2.1b). The increase in anisotropy led to further plasmon red-shifts for Ag triangular prisms (Fig. 2.1c) and Au octahedral (Fig. 2.1d), due to changes in the aspect ratio of the NPs. Nanoplates or triangular prisms have extremely large absorbing and scattering cross-sections across the visible and NIR regions of the spectrum. By precisely controlling the plate diameter and thickness, the SPR can be

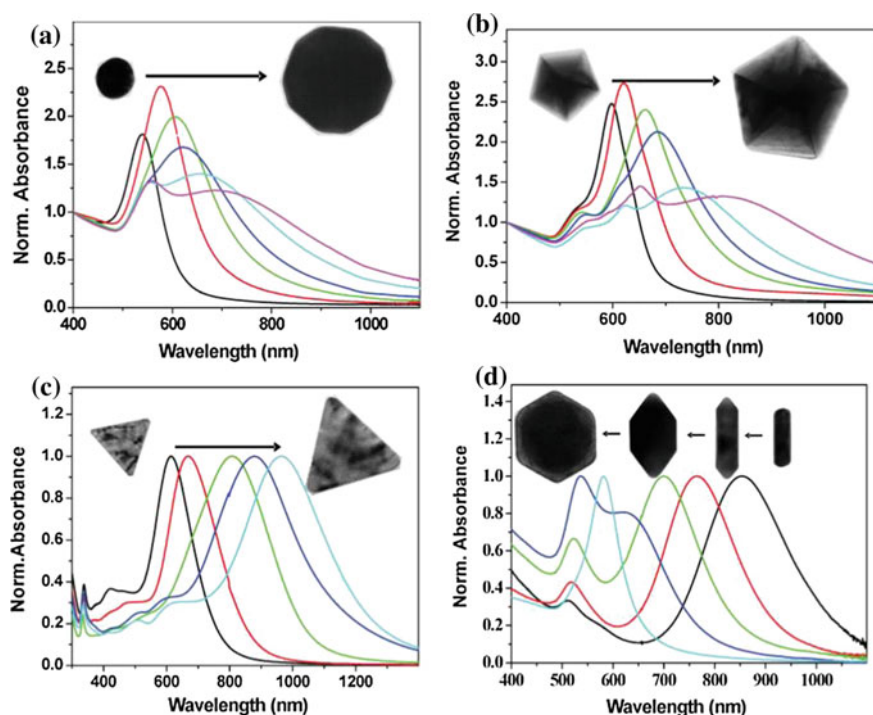


Fig. 2.2 UV-vis-NIR spectra of metal colloids with various morphologies and sizes. **a** Au spheres, **b** Au decahedra, **c** Ag nanoprisms and **d** transformation of Au nanorods into octahedra (Pastoriza-Santos and Liz-Marzán 2009)

tuned from 550–1100 nm. Nanoplates are generally coated with polyvinylpyrrolidone (PVP) as well as with silica shells for further bioconjugation.

2.2 Antimicrobial Silver Nanoparticles

Silver is known to have inhibitory and bactericidal effects. The antimicrobial effect of Ag dates back to the Greeks and Romans, who stored water in silver vessels. The release of Ag^+ ions from the container provides antimicrobial effect through Ag ion interaction with thiol groups of vital bacterial enzymes and proteins. This affects cellular respiration and transport of ions across membranes, resulting in cell death (Rai et al. 2009). Additional antimicrobial mechanistic pathways have also been proposed. The anchoring of Ag NPs and subsequent penetration of the bacterial cell wall (Sondi and Salopek-Sondi 2004) or generation of reactive oxygen species (ROS) would lead to DNA damage and structural changes on the cell membrane (Kim et al. 2007). While maintaining low toxicity of Ag for humans, the excellent antibacterial property has led

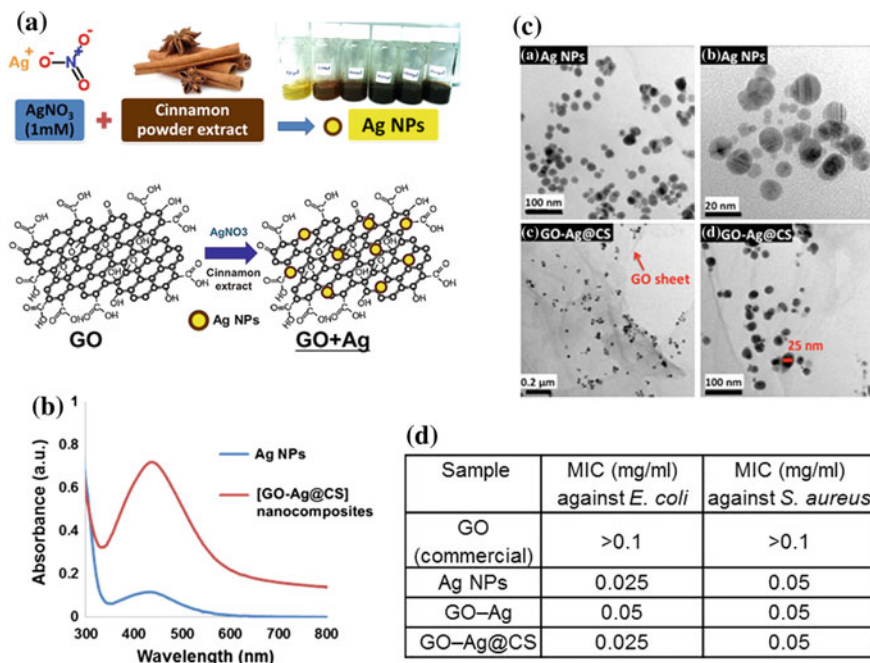


Fig. 2.3 Synthesis of Ag NPs (a), UV-vis absorption spectra of Ag NPs (b), TEM images of Ag NPs (c) and Antibacterial activity of different samples (d) GO graphene oxide, CS chitosan (Moosavi et al. 2015) (Copyright not required)

to the integration of Ag NPs in a wide variety of products including wound dressings, packaging materials, and antifouling surface coatings.

Very recently, we have demonstrated a facile method for the synthesis of Ag NPs using water-soluble plant extract of cinnamon as a green reducing and capping agent (Moosavi et al. 2015). The solution color changed from yellow to dark brown with an increase in cinnamon extract concentration indicating the formation of NPs (Fig. 2.3a). The formation of Ag NPs was confirmed by the surface plasmon resonance (SPR) absorption at 430 nm in the UV-vis spectra (Fig. 2.3b). Different nanocomposites of graphene oxide (GO) with only Ag [GO-Ag] and with Ag and chitosan (CS) [GO-Ag@CS] were also synthesized. TEM images (Fig. 2.3c) showed that the average diameter of Ag NPs is around 20–30 nm and they are uniform and evenly distributed on the GO sheet in the [GO-Ag@CS] nanocomposite. The antibacterial properties were evaluated by comparing the minimum inhibitory concentration (MIC) values for different samples against Gram-negative *E. coli* and Gram-positive *S. aureus* (Fig. 2.3d). The MIC values for both Ag NPs and nanocomposites against *E. coli* and *S. aureus* were 0.025 and 0.05 mg ml⁻¹, respectively. This method affords the advantages of reducing the usage of expensive Ag salts and NPs without compromising the antibacterial effect through the synergistic action of cinnamon and very low concentration of Ag salts used in our NPs

synthesis. Bi-functional nanocomposites exhibiting both antibacterial and magnetic properties can also be synthesized using this method.

2.3 Gold Nanoparticles for SERS Detection and Drug Delivery

The SERS based detection of Raman active molecules has been pioneered in the group of Liz-Marzán (Alvarez-Puebla and Liz-Marzán 2010; Contreras-Cáceres et al. 2010; Rodríguez-Lorenzo et al. 2009). Reduced graphene oxide (rGO) and noble metal NP hybrids have been extensively studied by different groups. It is worth mentioning here some of the notable achievements—for example, high aspect ratio Au nanostar/GO hybrids (Nergiz et al. 2014), direct growth of Au rods on graphene thin films (Kim et al. 2010), and the uses of GO hybrids for Raman detection of folic acid (Hu et al. 2013), and label-free SERS biosensing (Fan et al. 2013). GO-based nanocomposites were also used for anticancer drug, Doxorubicin loading and delivery (Yang et al. 2008, 2013).

Graphene and its derivatives such as reduced graphene oxide (rGO) have been used as substrates for the attachment of NPs and immobilization of drug molecules for ultrasensitive SERS detection and controlled drug delivery applications (Huang

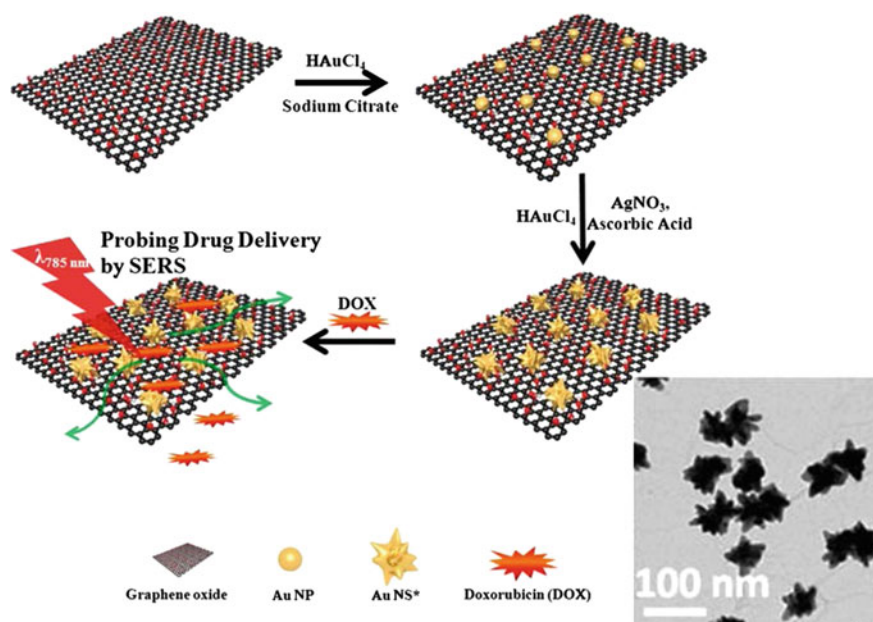


Fig. 2.4 Schematic illustration of the reduced graphene oxide-nanostar (rGO-NS) and TEM image of nanostars (Wang et al. 2014) (Copyright obtained)

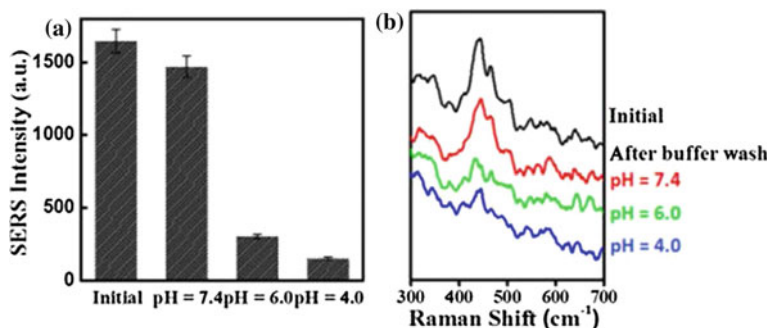


Fig. 2.5 SERS study on pH-dependent DOX release from rGO-NS. **a** SERS intensity after incubation with different pH buffers and **b** corresponding SERS spectra (Wang et al. 2014) (Copyright obtained)

et al. 2012; Wang et al. 2013; Xu et al. 2013). Reduced graphene oxide-gold nanostar (rGO-NS) nanocomposites were employed as active SERS materials for anticancer drug (doxorubicin, DOX) loading and release (Wang et al. 2014). The synthesis of these rGO-NS nanocomposites is shown schematically in Fig. 2.4. First, Au NPs were synthesized on the rGO colloidal solution by adding Au salt and the reducing agent, sodium citrate. Briefly, different amounts of the as-prepared rGO-NP seed solution were mixed with Au and Ag salts and ascorbic acid to form rGO-nanostar (rGO-NS) nanocomposites. Aromatic Raman active molecules such as mercaptobenzoic acid (MBA), crystal violet (CV), and doxorubicin (DOX), showed specific interactions and enhanced sensitivity with rGO-NS nanocomposites during Raman measurements under 785 nm laser excitation. The strongest SERS intensity for rGO-NS over either bare Au NS or rGO-NP seed was attributed to strong electromagnetic enhancement and nanoantenna effect. The authors have also shown that DOX release could be monitored by SERS (Fig. 2.5). The SERS measurements of rGO-NP-DOX solution indicated that ca. 90 % of the SERS signal was maintained at pH 7.4, whereas only 9 and 18 % were retained for pH 4.0 and 6.0, respectively. The more DOX release from rGO-NS under acidic conditions can be ascribed to the pH-dependent π - π stacking interaction between DOX and the aromatic domains of rGO.

2.4 Effects of Surface Functionalization of Au NPs on Cell Delivery

There have been a number of reviews delineating the recent advances in the field of drug delivery using Au NPs as carriers for therapeutic agents (Han et al. 2007; Huang et al. 2007). Functionalized Au NPs represent one of the promising candidates in the application of drug delivery owing to their unique dimensions,

controllable surface functionalities and drug release (Skrabalak et al. 2007). There are different ways by which Au NPs can be delivered into living cells. One such approach is the optical injection of Au NPs into living cells. The controlled injection of Au NPs into living cells with light offers promising prospects for the development of novel molecular delivery strategies or intracellular biosensor applications. Au NPs from solution were patterned on the surface of living cells with a continuous wave laser beam with a survival rate of >70 % (Yin et al. 2015). The Au NPs were used in different imaging modalities such as computed tomography (CT) imaging (Domey et al. 2015), SERS (Bu and Lee 2015; Yin et al. 2015), near-infrared imaging (Luo et al. 2015) and hyperthermia (Antosh et al. 2015) for theranostics. Antibody (anti-EGFR) modified Au NPs can be used to target efficiently the bladder cancer cell (Chen et al. 2015). Some of the efficient conjugating ligands and receptors for Au NPs are discussed in the following sections.

2.4.1 Au–Herceptin Nanoclusters for Nuclear Targeting and Cancer Therapy

High targeting specificity and nuclear localization capability are essential in the area of nuclear nanomedicine. Au NPs can be surface functionalized with different targeting ligands and receptors for cell internalization. The ligand, Herceptin possesses high targeting specificity and nuclear localization capability. The fluorescent Au nanoclusters (NCs) conjugated with Herceptin ligand induced nuclear damage and proposed to be useful for simultaneous imaging and enhanced cancer therapy (Wang et al. 2011). Importantly, it was concluded that the endocytosed Au–Herceptin nanoconjugates targeted the nucleus via the endolysosomal escape route, possibly due to its small size effect. This approach could be used to enhance the therapeutic effect of Herceptin.

Fluorescent correlation spectroscopy (FCS) and fluorescence lifetime imaging (FLIM) are powerful techniques in life science, which can be used to track the dynamics of nanoprobe at single particle sensitivity. A combination of FCS with FLIM was used to study the diffusion of Au–Herceptin conjugates and their entry into the nucleus in live cell conditions (Fig. 2.5). Fluorescence images of SKBR3 cells (Fig. 2.5a–c) treated with AuNCs (A), AuNCs–Her (B), and Herceptin (C) illustrated clearly the apoptosis induced by DNA damage because of the nuclear targeting ability of AuNCs–Her conjugates (Fig. 2.5b). Comparing AuNCs–Her (Fig. 2.5d) conjugates with Herceptin stained cells (Fig. 2.5e), it is clear that AuNCs–Her showed increased DNA damage, indicating the antitumor effect. Quantitative evaluation of DNA damage of cells indicated that only 35 % of the cells treated with Herceptin underwent apoptosis due to DNA damage compared to 95 % of the AuNCs–Her (Fig. 2.5f) treated cells, confirming the nuclear targeting efficiency and the antitumor activity of Herceptin–Au conjugates.

2.4.2 Au–Peptide NPs as Drug Delivery Vehicles

It has been shown that peptide capped Au NPs exhibited minimal cytotoxicity to mammalian HeLa and L929 cell lines as well as mice spleenocytes. Peptide capped Au NPs entrapping drugs were more efficient in killing HeLa cells compared to the free drug, exploring their use as alternate drug delivery vehicles (Parween et al. 2013). The drug resistance of cancer cells has become an important problem in therapeutic applications. Platinum-based chemotherapeutic agents such as cisplatin, oxaliplatin, and carboplatin are typical examples of anticancer drugs. However, these drugs may exhibit dose-dependent side effects to normal cells and drug resistance to cancer cells. To obviate these difficulties, nanocarrier based systems could be employed to enhance the specific targeting (therapeutic index) of cancer cells. Glutathione-stabilized gold (Au@GSH) NPs were used for the delivery of a platinum(IV) drug functionalized with the neuropilin-1 receptor (Nrp-1) -targeting peptide (CRGDK) to prostate cancer cells in vitro (Kumar et al. 2014). This approach led to enhanced cellular uptake level and cell toxicity through the specific

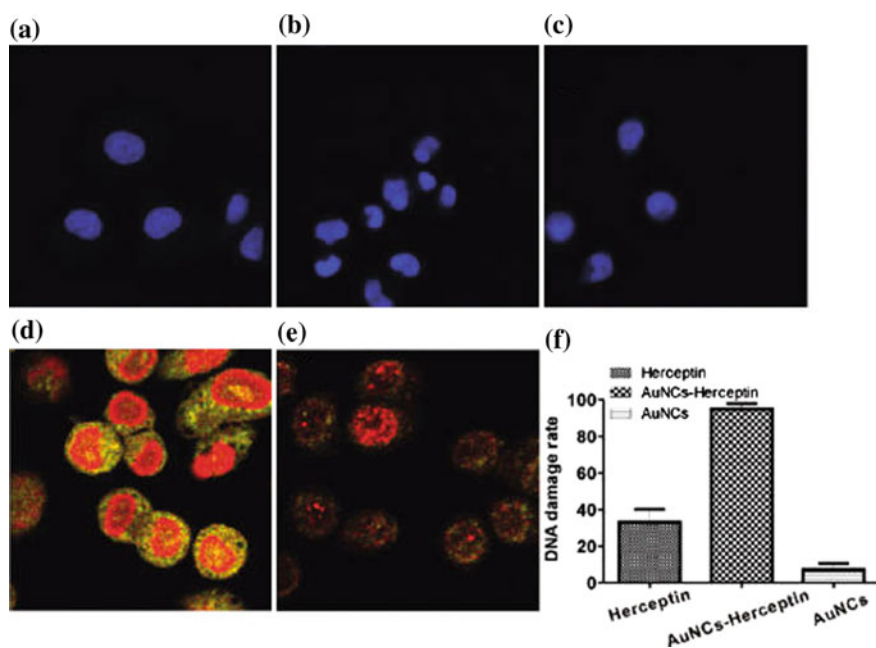


Fig. 2.6 Monitoring the apoptosis induced by AuNCs (a), AuNCs-Her (b), and Herceptin (c) with Hoechst 33258 staining. DNA damage of the cells was indicated by the bright yellow dots in SK-BR3 cells induced by AuNCs-Her (d) or Herceptin alone (e). Quantitative evaluation of DNA damage for different treatments (f) (Wang et al. 2011) (Copyright obtained)

binding of the peptide to the Nrp-1 receptor. Interestingly, these functionalized nanocarriers exhibited excellent anticancer activity, through the upregulation of nuclear factor kappa-B (NF- κ B) protein (p50 and p65) expression and activation of NF- κ B-DNA-binding activity.

The functionalization of Au@GSH gold NPs with Pt(IV) drug and the targeting peptide CRGDK is schematically illustrated in Fig. 2.6. The peptide conjugated

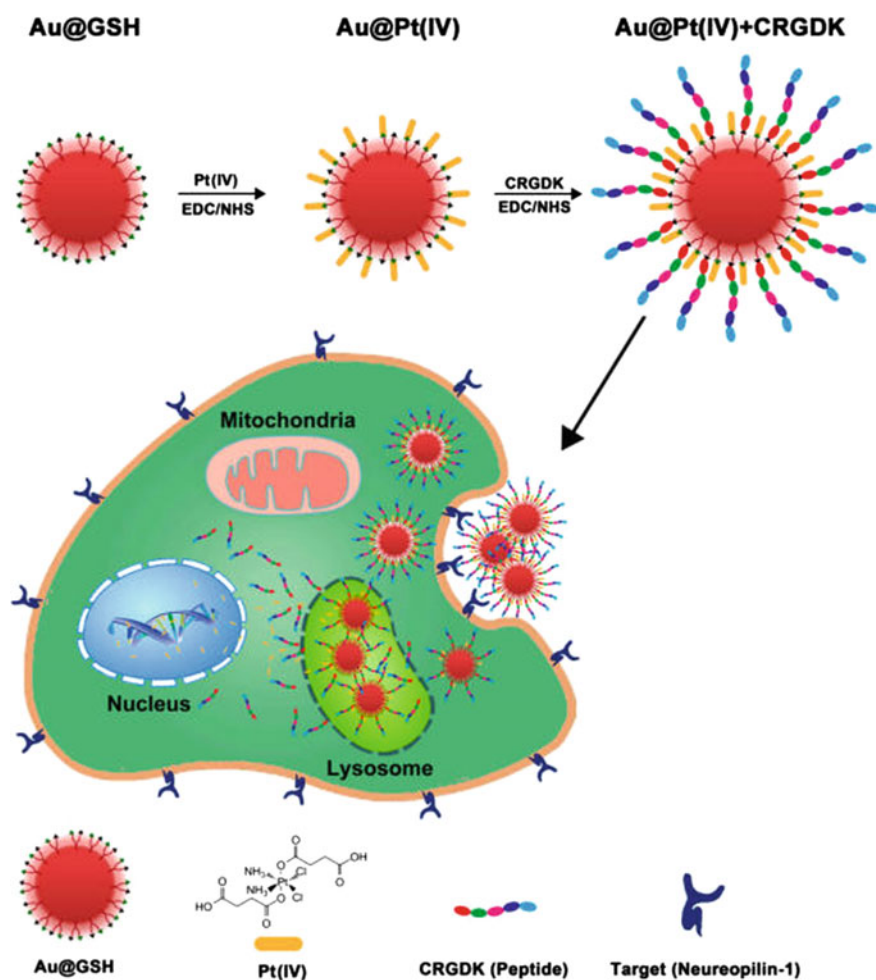


Fig. 2.7 Scheme for the functionalization of gold NPs with the chemotherapeutic drug and the targeting peptide for cancer treatment. Endocytosis mediated internalization of the NPs and delivery of the drug (Kumar et al. 2014) (Copyright obtained)

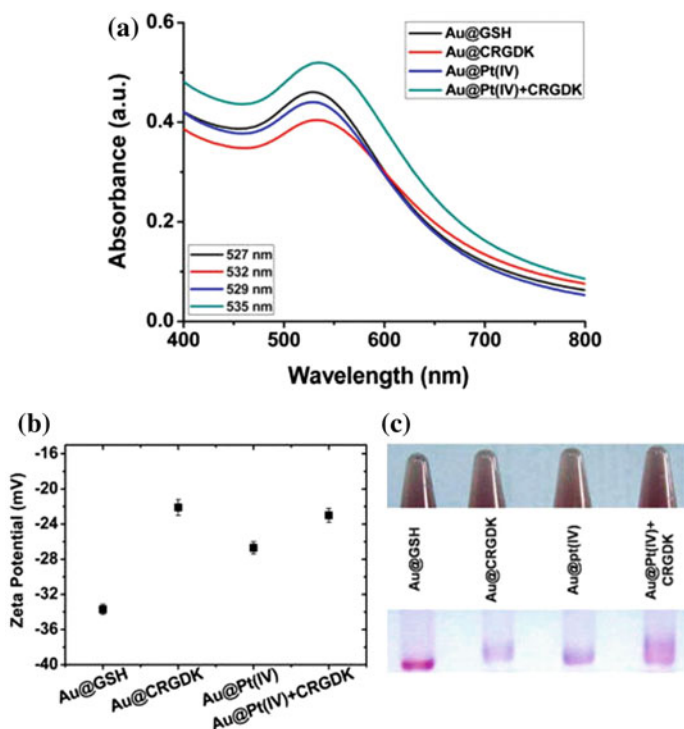


Fig. 2.8 **a** UV-vis spectra of the functionalized Au@GSH NPs. **b** Zeta potentials of the Au@GSH NPs and their functionalized products. **c** Qualitative assessment of the presence of peptide on the surface of NPs (Kumar et al. 2014) (Copyright obtained)

NPs enhanced the intracellular entry through the targeting of Nrp-1 receptor expressed on the human prostate cancer cells and internalized via receptor-mediated endocytosis. The surface plasmon band corresponding to Au@GSH NPs at 527 nm shifted to 535 nm for Au@Pt(IV)+CRGDK (Fig. 2.7a). On contrary, the zeta potential (Fig. 2.7b) of Au@Pt(IV)+CRGDK became less negative (-22.1 mV) compared to Au@GSH NPs (-33.7 mV). The conjugation of peptide to Au@GSH NPs was probed by agarose gel electrophoresis (Fig. 2.7c). The slow mobility observed for peptide and drug conjugated NPs compared to Au@GSH (unbound gold NPs), indicated the presence of peptide or drug on the surface of NPs. The presence of Pt(IV) on the surface of the NPs was confirmed by ICP-MS and by XPS (Kumar et al. 2014). The MTT cell viability assays and flow cytometry results for two different prostate cancer cells (PC-3 and DU-145) are shown in Fig. 2.8. Increased cytotoxicity and higher levels of apoptosis were observed for Au@Pt(IV)+CRGDK NPs, due to their superior uptake efficiency.

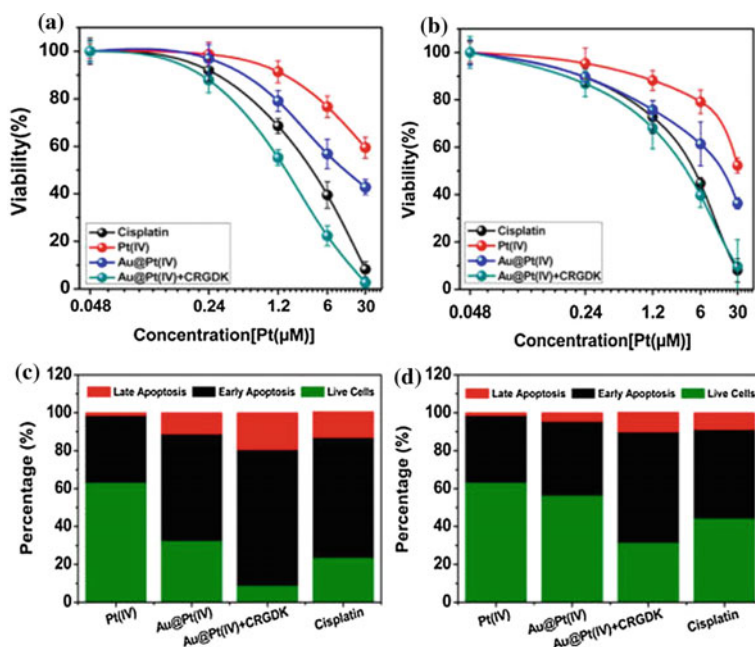


Fig. 2.9 MTT assays showing the cytotoxicity effects of cisplatin, platinum(IV), Au@Pt(IV) NPs, and Au@Pt(IV)+CRGDK NPs in PC-3 (a) and DU-145 (b) cells. Stages of apoptosis was verified in PC-3 (c) and DU-145 (d) (Kumar et al. 2014) (Copyright obtained)

2.5 Silver Nanoparticles for Photo-Activated Gene Silencing

Silver nanoparticles (SNPs) or Ag NPs with the size of 60–80 nm decorated with thiol-terminated photolabile DNA oligonucleotides were used as photo-activated drug delivery vectors (Brown et al. 2013). In vitro assays showed efficient photo-activation of surface-tethered caged ISIS2302 antisense oligonucleotides with internal photo-cleavable linkers (Fig. 2.9). These nanocarriers have several advantages such as protection against nucleases, efficient photorelease and enhanced cellular uptake when compared to commercial transfection agents. The light induced release of anti-sense oligonucleotides for silencing ICAM-1 (Intracellular Adhesion Molecule-1) has potential application in the wound healing, where inflammation is a major criterion such as in Crohn's disease (Figs. 2.10 and 2.11).

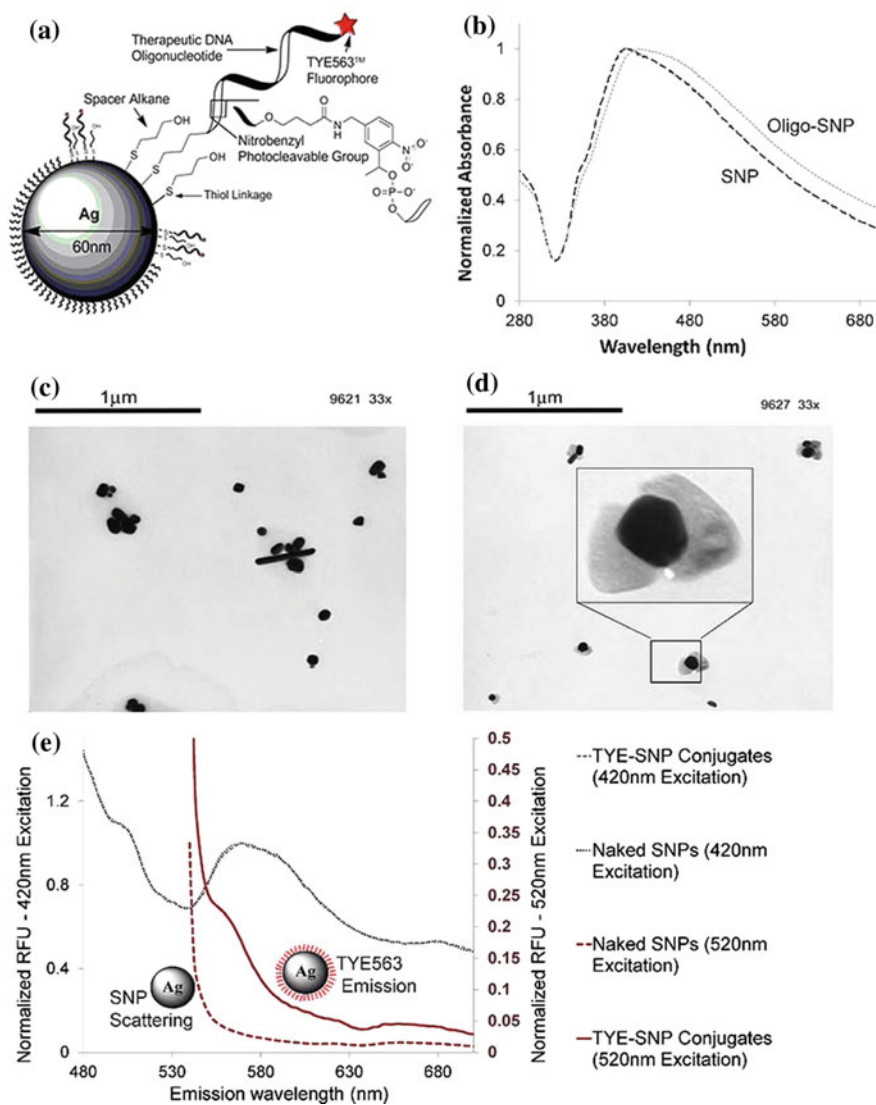


Fig. 2.10 Silver NPs and silver NP-oligo conjugates. **a** Functionalization with oligonucleotides. **b** Absorbance spectra for the NPs. **c** TEM images of the NPs ((c) for SNP and (d) oligo-SNPs). **e** Fluorimetry scans of NPs (Brown et al. 2013) (Copyright obtained)

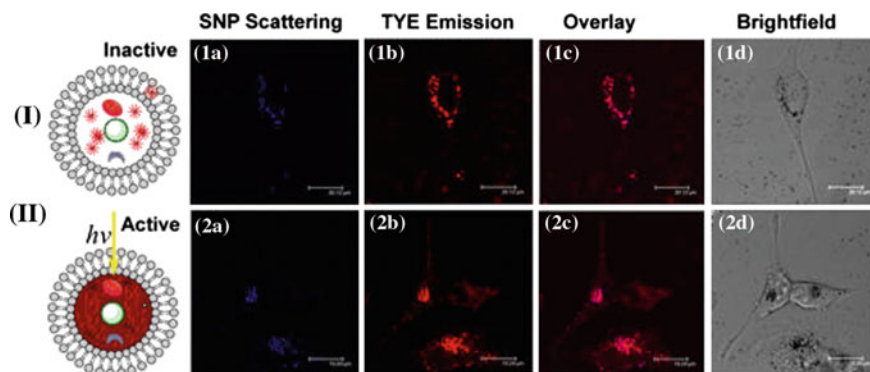


Fig. 2.11 Light induced delivery of oligonucleotides in cells. I. Schematic of intracellular **a** particle-bound oligonucleotide ligand vs **b** photoreleased ligand. II. (1) Nonreleased vs (2) photoreleased SNP-TYE-NPE(1n)-oligo conjugates samples. Images depict **a** particle scattering (488/488 nm), **b** TYE fluorescence (549/563 nm), **c** overlay, and **d** brightfield views (Brown et al. 2013) (Copyright obtained)

References

- Alvarez-Puebla RA, Liz-Marzán LM (2010) SERS-based diagnosis and biodetection. *Small* 6:604–610
- Antosh MP, Wijesinghe DD, Shrestha S, Lanou R, Huang YH, Hasselbacher T, Fox D, Neretti N, Sun S, Katenka N (2015) Enhancement of radiation effect on cancer cells by gold-pHLIP. *Proc Natl Acad Sci* 112:5372–5376
- Brown PK, Qureshi AT, Moll AN, Hayes DJ, Monroe WT (2013) Silver nanoscale antisense drug delivery system for photoactivated gene silencing. *ACS Nano* 7:2948–2959
- Bu Y, Lee S-W (2015) The characteristic AgcoreAushell nanoparticles as SERS substrates in detecting dopamine molecules at various pH ranges. *Int J Nanomed* 10:47
- Chen C-H, Chan T-M, Wu Y-J, Chen J-J (2015) Review: application of nanoparticles in urothelial cancer of the urinary bladder. *J Med Biol Eng* 35:419–427
- Contreras-Cáceres R, Pastoriza-Santos I, Alvarez-Puebla RA, Pérez-Juste J, Fernández-Barbero A, Liz-Marzán LM (2010) Growing Au/Ag nanoparticles within microgel colloids for improved surface-enhanced Raman scattering detection. *Chem A Eur J* 16:9462–9467
- Domey J, Teichgräber U, Hilger I (2015) Gold nanoparticles allow detection of early-stage edema in mice via computed tomography imaging. *Int J Nanomed* 10:3803
- Fan Z, Kanchanapally R, Ray PC (2013) Hybrid graphene oxide based ultrasensitive SERS probe for label-free biosensing. *J Phys Chem Lett* 4:3813–3818
- Han G, Ghosh P, Rotello VM (2007) Functionalized gold nanoparticles for drug delivery. *Nanomedicine* 2:113–123
- Hu C, Liu Y, Qin J, Nie G, Lei B, Xiao Y, Zheng M, Rong J (2013) Fabrication of reduced graphene oxide and silver nanoparticle hybrids for Raman detection of absorbed folic acid: a potential cancer diagnostic probe. *ACS Appl Mater Interfaces* 5:4760–4768
- Huang X, Jain PK, El-Sayed IH, El-Sayed MA (2007) Gold nanoparticles: interesting optical properties and recent applications in cancer diagnostics and therapy
- Huang X, Qi X, Boey F, Zhang H (2012) Graphene-based composites. *Chem Soc Rev* 41:666–686
- Kim H, Abdala AA, Macosko CW (2010) Graphene/polymer nanocomposites. *Macromolecules* 43:6515–6530

- Kim JS, Kuk E, Yu KN, Kim J-H, Park SJ, Lee HJ, Kim SH, Park YK, Park YH, Hwang C-Y et al (2007) Antimicrobial effects of silver nanoparticles. *Nanomed Nanotechnol Biol Med* 3:95–101
- Kumar A, Huo S, Zhang X, Liu J, Tan A, Li S, Jin S, Xue X, Zhao Y, Ji T (2014) Neuropilin-1-targeted gold nanoparticles enhance therapeutic efficacy of platinum (IV) drug for prostate cancer treatment. *ACS Nano* 8:4205–4220
- Luo H, Xu M, Zhu X, Zhao J, Man S, Zhang H (2015) Lung cancer cellular apoptosis induced by recombinant human endostatin gold nanoshell-mediated near-infrared thermal therapy. *Int J Clin Exp Med* 8:8758
- Moosavi R, Ramanathan S, Lee YY, Ling KCS, Afkhami A, Archunan G, Padmanabhan P, Gulyás B, Kakran M, Selvan ST (2015) Synthesis of antibacterial and magnetic nanocomposites by decorating graphene oxide surface with metal nanoparticles. *RSC Adv* 5:76442–76450
- Nergiz SZ, Gandra N, Tadepalli S, Singamaneni S (2014) Multifunctional hybrid nanopatches of graphene oxide and gold nanostars for ultraefficient photothermal cancer therapy. *ACS Appl Mater Interfaces* 6:16395–16402
- Nie S, Emory SR (1997) Probing single molecules and single nanoparticles by surface-enhanced Raman scattering. *Science* 275:1102–1106
- Parween S, Ali A, Chauhan VS (2013) Non-natural amino acids containing peptide-capped gold nanoparticles for drug delivery application. *ACS Appl Mater Interfaces* 5:6484–6493
- Pastoriza-Santos I, Liz-Marzán LM (2002) Synthesis of silver nanoprisms in DMF. *Nano Lett* 2:903–905
- Pastoriza-Santos I, Liz-Marzán LM (2009) N, N-dimethylformamide as a reaction medium for metal nanoparticle synthesis. *Adv Funct Mater* 19:679–688
- Rai M, Yadav A, Gade A (2009) Silver nanoparticles as a new generation of antimicrobials. *Biotechnol Adv* 27:76–83
- Rodríguez-Lorenzo L, Alvarez-Puebla RA, Pastoriza-Santos I, Mazzucco S, Stéphan O, Kociak M, Liz-Marzán LM, García de Abajo FJ (2009) Zeptomol detection through controlled ultrasensitive surface-enhanced Raman scattering. *J Am Chem Soc* 131:4616–4618
- Skrabalak SE, Au L, Lu X, Li X, Xia Y (2007) Gold nanocages for cancer detection and treatment. *Nanomedicine* 2:657–668
- Sondi I, Salopek-Sondi B (2004) Silver nanoparticles as antimicrobial agent: a case study on *E. coli* as a model for Gram-negative bacteria. *J Colloid Interface Sci* 275:177–182
- Wang P, Zhang D, Zhang L, Fang Y (2013) The SERS study of graphene deposited by gold nanoparticles with 785 nm excitation. *Chem Phys Lett* 556:146–150
- Wang Y, Chen J, Irudayaraj J (2011) Nuclear targeting dynamics of gold nanoclusters for enhanced therapy of HER2 + breast cancer. *ACS Nano* 5:9718–9725
- Wang Y, Polavarapu L, Liz-Marzán LM (2014) Reduced graphene oxide-supported gold nanostars for improved SERS sensing and drug delivery. *ACS Appl Mater Interfaces* 6:21798–21805
- Xu W, Mao N, Zhang J (2013) Graphene: a platform for surface-enhanced Raman spectroscopy. *Small* 9:1206–1224
- Yang X, Zhang X, Liu Z, Ma Y, Huang Y, Chen Y (2008) High-efficiency loading and controlled release of doxorubicin hydrochloride on graphene oxide. *J Phys Chem C* 112:17554–17558
- Yang Y, Asiri AM, Tang Z, Du D, Lin Y (2013) Graphene based materials for biomedical applications. *Mater Today* 16:365–373
- Yin HJ, Chen ZY, Zhao YM, Lv MY, Shi CA, Wu ZL, Zhang X, Liu L, Wang ML, Xu HJ (2015) Ag@ Au core-shell dendrites: a stable, reusable and sensitive surface enhanced Raman scattering substrate. *Scientific reports* vol 5
- Yu D, Yam VW-W (2005) Hydrothermal-induced assembly of colloidal silver spheres into various nanoparticles on the basis of HTAB-modified silver mirror reaction. *J Phys Chem B* 109:5497–5503

Introduction to Nanotheranostics

Tamil Selvan, S.; Narayanan, K.

2016, VII, 79 p. 47 illus., 39 illus. in color., Softcover

ISBN: 978-981-10-1006-4